Sensors and Materials, Vol. 37, No. 8 (2025) 3633–3649
MYU Tokyo

S & M 4142

Thermal Hazard Alarm System in Wind Turbines Based on Nanoparticle Detection

Fuhao Du,* Lun Liu, and Man Xu

Wuhan Cloud Scout Science & Technology Co., Ltd. Wuhan 430073, China

(Received May 6, 2025; accepted July 31, 2025)

Keywords: thermal hazard, nanoparticle, wind turbines, device

The early fire warning of a wind turbine is very important to ensure its safe operation and maintenance. We developed a thermal hazard sensing device based on thermally released nanoparticles, by which the early fire of wind turbine electrical equipment can be found promptly. We first introduce commonly used methods for very early fire warning in power systems, analyze the thermal pyrolysis process of cables, and propose a detection approach for identifying thermal hazards by monitoring characteristic nanoparticles released during the thermal pyrolysis of hazardous materials. For detecting the nanoparticles emitted during the thermal pyrolysis of hazardous materials in wind turbines, experimental platforms were established. Combustion experiments were conducted on representative fire-prone materials generally used in wind turbines. From the results of these experiments, the characteristic nanoparticles associated with thermal hazards in wind turbines and their detection alarm thresholds were determined. On the basis of these findings, the device was developed and subjected to detection performance tests and anti-interference tests against water mist and dust. The developed device is currently applied in early fire warning systems for wind turbines, demonstrating its effective performance.

1. Introduction

With the rapid development of new energy power generation technologies, the newly added wind power capacity installed globally reached 121.6 GW in 2024, marking a 3.9% increase compared with 2023. As more wind turbines are commissioned and their operational lifespans extend, the probability and frequency of wind turbine accidents have steadily risen. Among these incidents, fire accidents account for a significant proportion and result in substantial economic losses. The distribution of global wind turbine accidents from 2020 to March 2023, obtained from statistical data, is shown in Fig. 1.[1] As shown in Fig. 1, blade failures constitute the highest proportion (15%), followed by fire accidents (14%).

The causes of wind turbine fires typically include the following: (a) Electrical equipment failures leading to fires:[2–8] These include insufficient insulation protection measures for electrical equipment connection points and exposed busbars, loose bolts in electrical equipment

*Corresponding author: e-mail: 13971150995@163.com
https://doi.org/10.18494/SAM5726

ISSN 0914-4935

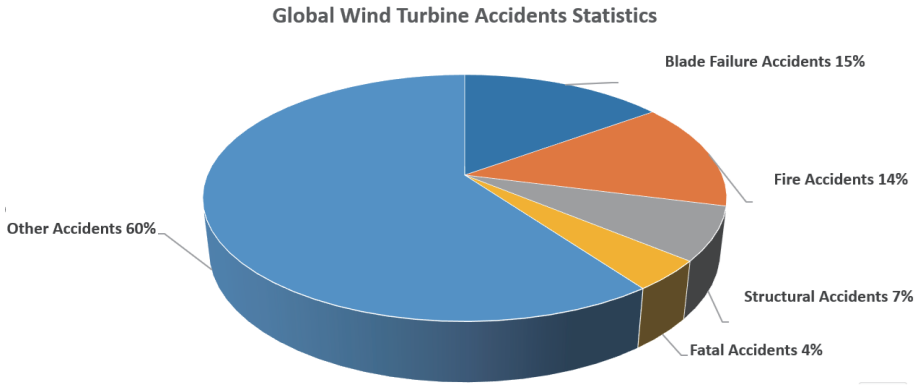

Fig. 1. (Color online) Global wind turbine accident statistics.

connections, and an improper configuration of electrical circuit protection systems within the turbine. (b) Lightning strikes causing fires:[2] These include poor contact in the turbine's lightning protection grounding circuits and noncompliant grounding resistance or inadequate lightning arrestor pathways in the turbine. (c) Mechanical failures resulting in fires:[3] These include an abnormal pitching mechanism, which prevents the proper feathering of blades, the abnormal vibration of the generator, which causes discharge between slip rings and carbon brushes, and incomplete protective covers for mechanical brakes with flammable materials present beneath them. (d) Human operational and maintenance errors:[4] These include the improper adjustment of brake clearance during mechanical brake system operations, the repeated forced reset of turbine faults without identifying the root cause, failure to tighten bolts to the required torque after replacing electrical equipment, and the untimely removal of oil stains and debris inside the turbine, leading to fires due to improper maintenance practices.

Given the vast scale of wind farms and the distance between turbines and operation and maintenance stations, the absence of real-time safety monitoring systems may delay the detection of potential hazards, resulting in their escalation into full-scale accidents. Furthermore, once a turbine catches fire, repair crews often struggle to reach the site promptly. The turbine's height and confined internal spaces render conventional fire-extinguishing equipment ineffective, frequently leading to the total destruction of the turbine and massive economic losses. Therefore, the early detection and timely warning of wind turbine fires play a crucial role in ensuring the safe operation of wind turbines.

Presently, there is limited research on how to detect wind turbine fire incidents very early. Sun *et al.* studied the thermal hazards and decomposition characteristics caused by temperature variations for wind turbine oil systems.[6] They pointed out that the thermal decomposition of the lubricating and transformer oils can be divided into three stages, with major mass loss in the second stage. Rengel *et al.* carried out a computational fluid dynamics simulation to estimate the effects during the first minutes of a typical wind turbine fire in an electrical cabinet and reported about how a fire develops inside a wind turbine.[7] Wan *et al.* used the Extree Gradient Boosting Tree algorithm to build an offshore wind turbine unit fire detection model with a multiparameter, which is based on the wind turbine operation data in a Supervisory Control and Data Acquisition

system.[8] Kim *et al.* analyzed real-time wind speed, direction, and temperature, then used fuzzy rules and data mining cluster analysis techniques to prevent turbine fires.[4]

Regarding the early detection of electrical fires, there are some promising and significant studies currently focused on fire detection in cables. Some methods utilize characteristic objects emitted during the early or latent stages of a fire to achieve early warning. During the early stages of a fire and in latent hazard phases, overheated cables will decompose and emit characteristic by-products, whose detection can trigger warnings at the very earliest phases of a potential fire. Zhou *et al.* proposed that polyethylene cable fire can be detected early by monitoring the ratio of CO to CO_2 generated by the pyrolysis of the outer sheath of the cable.[9] Han *et al.*[10] and Yi *et al.*[11] found that semivolatile dioctyl phthalate and 2-ethylhexanol were the major volatile species in vapors from overheated PVC cables, and detected them as potential fire signatures using metal oxide gas sensors. Xiong *et al.* pointed out that the concentration of volatile organic compounds (VOCs) during the thermal degradation of the busway insulating layer can be used for judging an overheating fault, and they developed an overheating fault alarm system for busways in buildings using the AdaBoost classifier method.[12] Wang *et al.* designed an early fire warning system by identifying the volatile gases emitted from overheated materials in electrical equipment at different heating stages by integrating the Global Extension Extreme Learning Machine.[13] Fu *et al.* proposed that the count of emission particles with specific diameters and the concentration of VOCs can be used as criteria for discovering fire hazards in power cable tunnels, then presented a fire hazard alarm method that involved the monitoring of the concentration trends of VOCs and particles.[14]

Other methods utilize a combination of multiple features to identify early fires. Li *et al.* analyzed the temperature distribution and characteristic gas concentration under different simulation conditions, and proposed a fire early warning method for a high-voltage power cable involving the monitoring of temperature, flue gas concentration, and CO and CO_2 concentrations.[15] Chen *et al.* investigated the effects of overcurrent, damage, aging, and environmental temperature on the risks of early cable fires caused by overload, and presented a hybrid fire risk assessment model for the early warning of cable fires.[16] Li *et al.* used Faster-Region-based Convolutional Neural Networks (RCNNs) to extract image features and fuse them with ambient temperature and volatile data, then made a fire warning model using Support Vector Machine (SVM) for intensive insulated busways in buildings.[17]

The aforementioned studies primarily focused on early warning for fires, with some research employing feature gas monitoring to warn against cable overheating or fire hazards.[10–14] In this study, the innovation lies in proposing online monitoring thermal hazard technology for wind farm turbines and their internal electrical equipment. Through monitoring the nanoparticles emitted, this technology enables the real-time monitoring of safety hazards such as equipment overheating, cable heating, component overheating, and discharge from insulation defects within the turbine. An experimental platform was established to conduct extensive experiments aimed at identifying and characterizing the concentration characteristics of nanoparticles emitted from fire-prone materials in wind turbines under heating conditions. Through experiments, nanoparticle detection alarm thresholds for different hazard locations in wind turbines were obtained. On the basis of these studies, a warning device for detecting thermal hazards in wind

turbines was developed and tested, which can enhance the overall safety management level of wind farms by enabling early intervention and reducing accident risks.

2. Warning Mechanisms for Wind Turbine Thermal Hazards

2.1 Causes and development stages of wind turbine fires

Modern large-capacity wind turbines have high load densities. Over time, as the turbine nacelles operate, the wear and tear of system components occur, leading to aging electrical components with increased contact resistance. The confined and densely packed internal space of the nacelles impedes smoke and heat dissipation, making it highly susceptible to fires when temperatures exceed ignition points. Additionally, wind turbines are often installed on elevated slopes and are typically the tallest structures in their vicinity, making them vulnerable to lightning strikes—a major threat to their safe operation. If lightning currents are not safely discharged after striking turbine blades, electrical components may be damaged or overheat, potentially causing lubricant temperatures to rise and ignite, ultimately leading to fires.

Among the numerous thermal hazards in wind turbine systems, flammable materials prone to combustion include thermal insulation foam in nacelles, plastic nacelle cover insulation layers, cable insulation materials, and lubricant leaks. The combustion of these flammable materials can be divided into three phases: thermal degradation, smoldering, and flaming, as illustrated in Fig. 2.

(a) Thermal Degradation Stage

Under heat sources, the portion of flammable materials closest to the heat source undergoes rapid temperature increases and initiates pyrolysis reactions. Heat is conducted inward,

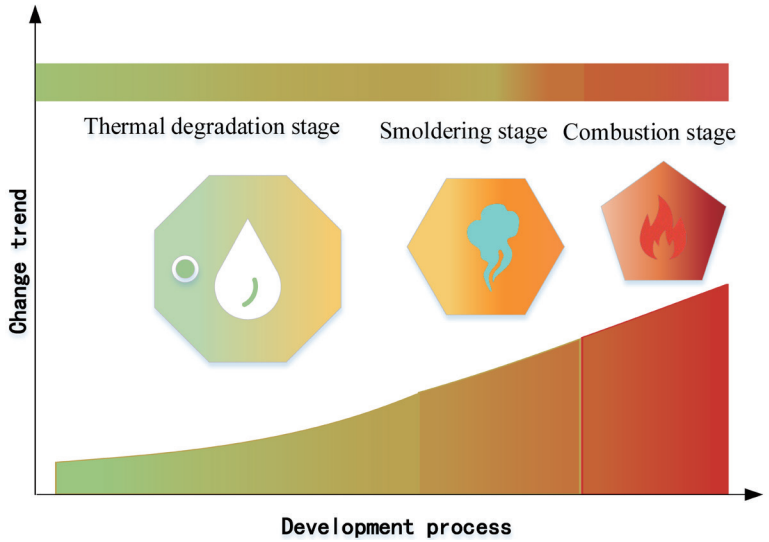

Fig. 2. (Color online) Three stages of combustion of flammable materials.

gradually triggering further pyrolysis and releasing various volatile gases. These gases include both combustible and noncombustible components, along with soot nanoparticles.

(b) Smoldering Stage

The gases interact with air at the gas–solid interface, undergoing gas-phase oxidation reactions that release heat. During the smoldering stage, smoke will gradually be produced.

(c) Flaming Stage

As temperatures continue to rise and smoke concentrations increase, cables begin to ignite and produce visible flames.

2.2 Thermal hazard warning for wind turbines based on nanoparticle detection

2.2.1 Thermal pyrolysis of fire hazard materials

When heated, thermal hazard materials undergo thermal decomposition and release a series of by-products as the temperature increases. Taking power cables as an example, Pu *et al.* studied the mass loss curve of a cable during thermal pyrolysis, and some of their experimental data are shown in Fig. 3.[18]

Under constant heating, the pyrolysis of a cable (with layered materials) undergoes temperature increases; pyrolysis is governed by the Arrhenius equation, resulting in continuous mass loss. Once the temperature stabilizes, pyrolysis peaks at 0.3 g/s at around 10 s. Subsequently, the surface mass density decreases and the pyrolysis rate gradually decreases. As cable mass diminishes, the pyrolysis continues with insulation and sheath layer degradation after 30 s, maintaining a mass loss rate of ~0.15 g/s until 50 s. Only minimal cable remnants remain by 60 s, with the pyrolysis rate dropping to 0.01 g/s.

The mass loss rate of the solid phase directly correlates with the heat release rate, as thermal energy converts solid-phase materials into gaseous fuels that combust in the gas phase. For cable joints and wiring materials (with compositions similar to power cables), similar solid-phase

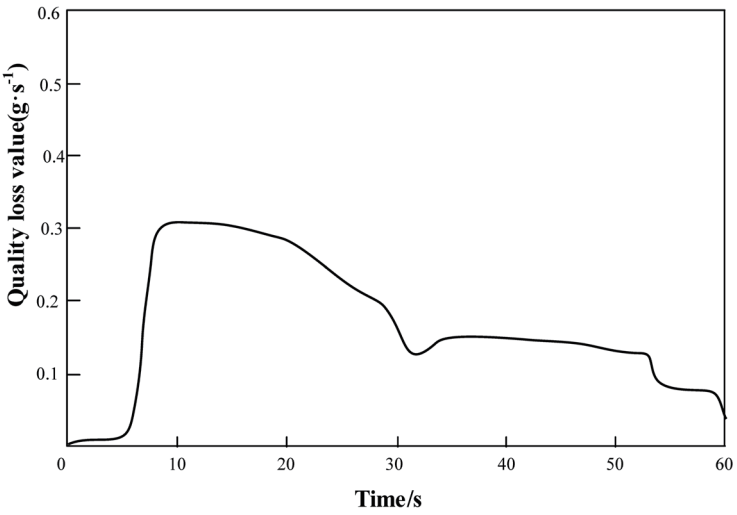

Fig. 3. Mass loss rate of cables during thermal pyrolysis.

pyrolysis occurs during the early heating stages, leading to mass loss. Thus, monitoring solid-phase pyrolysis by-products near electrical equipment in wind turbines enables the establishment of a relationship between equipment safety hazards and pyrolysis by-products, enabling the assessment of thermal hazards within nacelles.

2.2.2 Nanoparticle detection

Smoke particles typically range from 10 to 650 nm in diameter, and airborne dust and PM2.5 particles are generally smaller than 2.5 μm (2500 nm).[19] However, early-stage thermally released particles have diameters of 2–20 nm, with no overlap in size distribution with the aforementioned particles.[19]

By detecting these early-stage thermally released nanoparticles (which are distinct from smoke and dust), interferences from smoke and particulate matter can be avoided for the system, achieving zero false alarms. This enables the earliest possible detection of thermal hazards and the issuance of warnings.

When no thermal hazard exists, the nanoparticle concentration in a sealed clean environment remains relatively constant. However, when materials reach the critical point of a thermal hazard, the concentration of thermally released nanoparticles sharply increases. On the basis of the Mie scattering theory, the light beams scattered by nanoparticles can be measured.[20] By calculating the incident and scattered light intensities before and after nanoparticle interaction, we can determine the number of thermally released nanoparticles. This enables the accurate assessment of fire conditions based on nanoparticle concentration trends and nanoparticle evolution.[19]

When the particle concentration is N, the angular scattered light intensity is given by

$$I(\theta) = N\frac{\pi^4 d^6}{8\lambda^4 r^2}\left(\frac{m^2-1}{m^2+2}\right)^2\left(1+\cos^2\theta\right)I_0. \tag{1}$$

Here, θ is the scattering angle, $I(\theta)$ is the scattered light intensity when $\theta = 0$, λ is the wavelength of the light source, I_0 is the incident light intensity, d is the particle diameter, m is the refractive index of light, and r is the distance from a scattering particle. During detection, the parameters λ, I_0, d, m, and r are considered to remain constant. Thus, a constant C can be defined as

$$C = \frac{\pi^4 d^6}{8\lambda^4 r^2}\left(\frac{m^2-1}{m^2+2}\right)^2 I_0. \tag{2}$$

Therefore, the relationship between N and $I(\theta)$ can be expressed as

$$I(\theta) = NC(1+\cos^2\theta). \tag{3}$$

In practice, to simplify the computational complexity, the scattered light is typically measured over a solid angle (approximating the scattering angle θ as a fixed value of 0^0). This makes the received scattered light intensity approximately proportional to the particle concentration. Consequently, this approach enables the precise tracking of the concentration trends of thermally released nanoparticles, facilitating the detection of thermal hazards.

2.3 Analysis of thermal hazards leading to fire risks in wind turbines

In wind turbine systems, several critical thermal hazards that may lead to fire incidents involve flammable materials such as thermal insulation foam materials inside nacelles, plastic insulation layers of nacelle cover, cable insulation materials, and leaked lubricants. To study these fire risks, experimental setups were constructed to simulate the process of thermal-hazard-induced fires, the concentration of thermally released nanoparticles generated during experiments was detected, and its correlation with thermal hazards was analyzed.

3. Experimental Detection of Wind Turbine Thermal Hazards

3.1 Experimental design

Under laboratory conditions, a series of thermal hazard fire by-product simulation experiments were conducted on representative materials from wind turbine electrical equipment. These experiments simulated fire scenarios by continuously heating materials to their ignition temperatures using a temperature-controlled electric heating platform. Dust particle counters were employed to monitor in real time the particle concentration (by diameter) in the experimental environment. The selected test samples included thermal insulation foam materials (glass fiber felt) from turbine nacelles, polyurethane foam, the glass-fiber-reinforced plastic (GFRP) used in nacelle cover insulation layers, and lubricating oils.

The samples were placed on an electric heating platform to conduct a simulated combustion experiment, as shown in Fig. 4. The temperatures of the samples were uniformly and slowly increased from room temperature to 250 °C. During heating, the thermally released nanoparticle concentration increased, accompanied by smoke generation, and the particle detector parameters rose. An alarm was triggered approximately 1 min before visible smoke emission. Upon reaching 250 °C and ceasing heating, the nanoparticle concentration peaked.

3.2 Experimental results

3.2.1 Particle concentration observations

During the experiment, the number of particles in the environment was measured in real time using a laser particle counter (model CLJ-3016). The comprehensive analysis of the particle count data exported from the counter provided the numbers of particles with sizes of 0.3 μm (<0.3 μm), 0.5 μm (0.3–0.5 μm), 1.0 μm (0.5–1.0 μm), 3.0 μm (1.0–3.0 μm), 5.0 μm (3.0–5.0 μm),

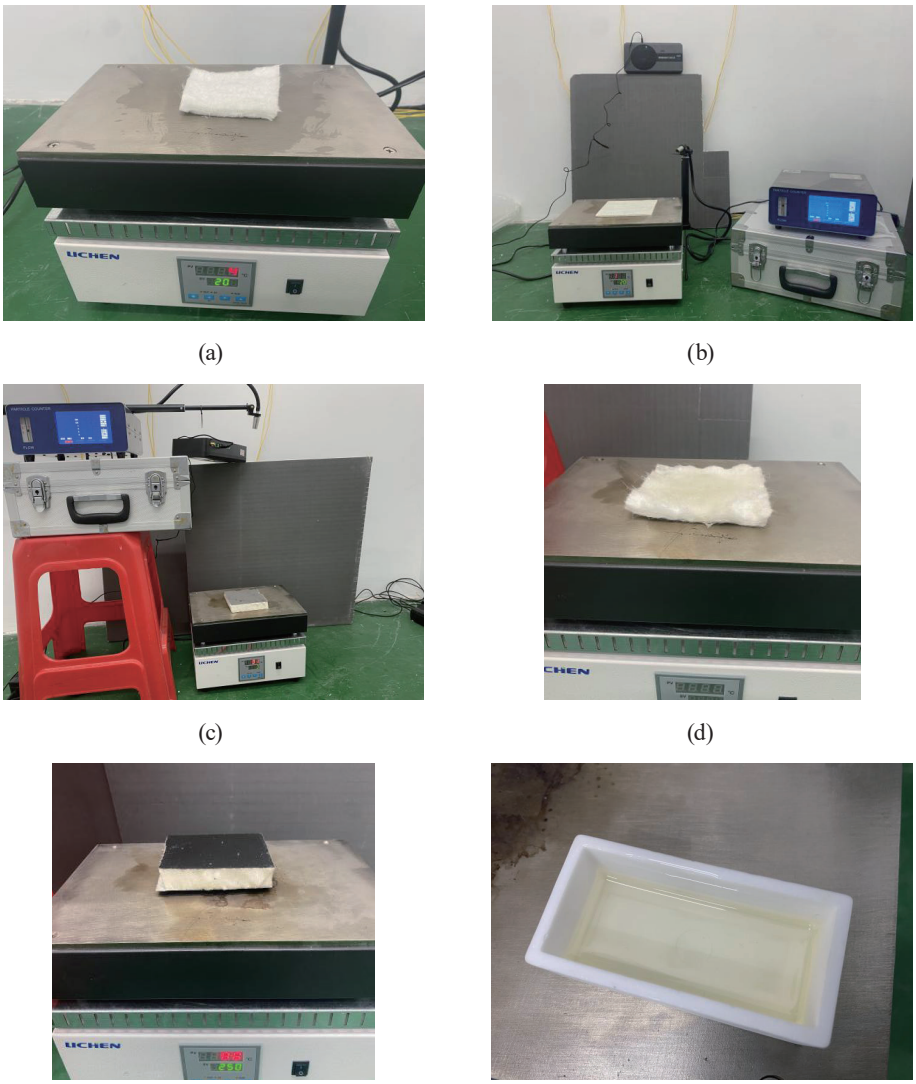

Fig. 4. (Color online) Simulations of combustion experiments. (a) glass fiber felt, (b) GFRP, (c) polyurethane panel, (d) oil-impregnated glass fiber felt, (e) oil-impregnated polyurethane panel, and (f) lubricating oil.

and 10.0 μm (5.0–10.0 μm). These data were used to plot concentration variation curves for particles of different diameters. Taking the simulated combustion experiment of the polyurethane panel as an example, the results are shown in Fig. 5.

By analyzing particle concentration variations at different particle diameters from the above polyurethane panel combustion experiment, we can draw the following conclusions:

(a) Particle size distribution observations

During the experiment, the highest concentrations were observed for nanoparticles with diameters of 0.3 and 0.5 μm. Smaller numbers of 1.0- and 3.0-μm-diameter particles were also detected, whereas particles of 5.0 and 10.0 μm diameters were scarcely observed.

(b) Temperature-dependent particle generation

As the temperature increased, particle generation began at a specific threshold. The concentrations of the 0.3- and 0.5-μm-diameter particles steadily increased with further

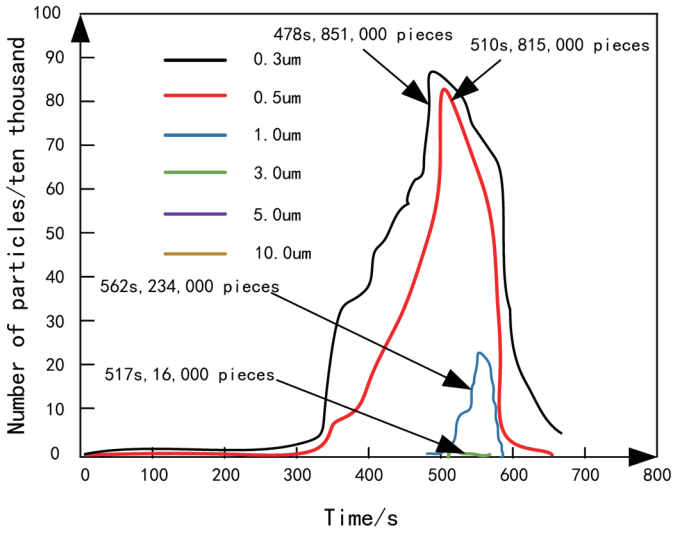

Fig. 5. (Color online) Concentration variations of particles of different diameters.

heating. At higher temperatures, a very small number of 1.0-μm-diameter particles were detected. When heating ceased, particle concentrations reached their peak across all sizes. Subsequently, as the temperature decreased to ambient levels, the number of particles diminished. This demonstrates a positive correlation between particle concentration and temperature.

Thus, it was concluded that the numbers of 0.3- and 0.5-μm-diameter particles detected during polyurethane panel combustion can serve as characteristic parameters for fire warning in wind turbine systems. These nanoparticles are proposed as key detection targets for thermal hazard monitoring and early fire warning systems in wind farms.

3.2.2 Experimental results

As shown in Table 1, the results were obtained through the experiments described in Sect. 3.1.

The analysis of the data in Table 1 reveals the following: Particles with diameters smaller than 0.3 μm are universally generated across simulations of combustion experiments for various materials. Their concentration changes exhibit a positive correlation with temperature increases. Therefore, selecting a particle diameter smaller than 0.3 μm as one of the environmental safety characteristic parameters for wind turbines is highly practical.

From the results of analysis and comparison of the generation patterns of particles smaller than 0.3 μm in diameter across simulations of different combustible materials, it is recommended to set the alarm threshold for particles smaller than 0.3 μm in diameter at 100,000 particles (equivalent to the peak values from glass fiber felt combustion).

In conclusion, according to the results of experimental validation and analysis in this study, the *what* of particles with diameters smaller than 0.3 μm can be adopted as an environmental safety characteristic parameter for wind farms. A wind farm fire monitoring and early warning

Table 1
Recommended alarm thresholds.

Location in turbine	Material	Particle diameter (μm)	Peak value (10000 pieces)	Recommended threshold
Soundproofing foam	glass fiber felt	0.3	13.7	10
		0.5	1.4	—
Nacelle cover	GPFR	0.3	53.4	40
		0.5	22.4	—
Thermal insulation layer	polyurethane panel	0.3	85.1	60
		0.5	81.5	—
		1	23.4	—
		3	1.6	—
Soundproofing foam	oil-immersed glass fiber felt	0.3	66.1	50
		0.5	47.3	—
Thermal insulation layer	oil-immersed polyurethane panel	0.3	80.0	60
		0.5	72.7	—
		1	10.5	—

model can thus be established to provide proactive thermal hazard warnings for wind farm operations.

4. Development of Thermal Hazard Monitoring Device

4.1 Hardware design

Currently, there are several solid-state particle detection technologies, including diffraction scattering,[21] angular scattering,[22] full scattering,[23] laser holography,[24] and dynamic light scattering (DLS).[25] In this study, we aimed to develop a device capable of measuring solid particles with diameters ranging from 0.1 to 10 μm. DLS can meet particle size requirements, but it requires a liquid medium for detection. Laser holographic scattering involves expensive equipment, making it impractical. In the case of the angular and full scattering methods, the minimum particle sizes they can detect are too large to satisfy our early-stage detection needs.

On the basis of prior analysis, we adopted the Mie scattering theory to design a particle detection module. To enhance detection precision, the environmental gas containing particles is first subjected to size amplification preprocessing (particle size enhancement) before being analyzed by the detection module.

According to the Mie scattering theory, to detect solid particles of 0.1–10 μm diameter, the wavelength of the detection laser beam must be smaller than 1 μm. Under these conditions, the scattering process aligns fully with theoretical predictions. The thermal hazard monitoring device for wind turbines operates as follows:

a) Air sampling: Air containing solid particles is collected.
b) Laser illumination: A specific laser beam illuminates particles as they pass through a light-sensitive region.
c) Scattering and signal conversion: Particles scatter light pulses proportional to their size; these signals are captured by photodetectors, converted into electrical pulse signals, and amplified.

d) Data analysis: The number of particles per liter (pcs/L) is calculated by counting electrical pulses over a detection cycle, then algorithms convert this count into mass concentration (μg/m^3).
e) Module design: By analyzing the relationship between scattered light intensity and scattering angle, a thermally released nanoparticle detection module is designed on the basis of Mie scattering principles.

The system employs the optical setup shown in Fig. 6, comprising the following components arranged sequentially: semiconductor laser source (light source), collimating lens (to form a parallel beam), multistage grating (for beam modulation), detection zone (particle–laser interaction region), and extinction structure (to suppress stray light). A light-receiving structure (photodetector array) is positioned at the end of the light-sensitive region. This structure measures light intensity fluctuations caused by particles in the detection zone, converts these signals into electrical outputs, and provides foundational data for the real-time quantification of particle concentration.

In addition to the optical path configuration, the particle detection module designed in this study includes a structurally compatible housing and a circuit board tailored to integrate with the optical system. Both the semiconductor laser source and photodetectors are mounted on the printed circuit board (PCB). A signal amplification circuit is also integrated to amplify the electrical signals captured by the photodetectors, enabling efficient data processing. The structural housing ensures precise alignment between the optical components (laser source, lenses, and gratings) and the detection zone. The PCB consolidates all electronic functionalities, forming a complete thermal hazard detection module that seamlessly combines optical sensing, signal processing, and output capabilities.

4.2 Device tests

4.2.1 Particle detection experiment

The experiment on the performance of our developed particle detection module primarily utilizes a standard smoke chamber to simulate thermally released nanoparticles emitted from target materials. The performance of the sensor unit is validated by comparing and analyzing the measured parameters obtained from the sensor unit.

In this experiment, owing to the similarity in size between solid-state particles and aerosols, a standard smoke chamber (model: ZB-SMK-I) was selected to simulate the emission of solid

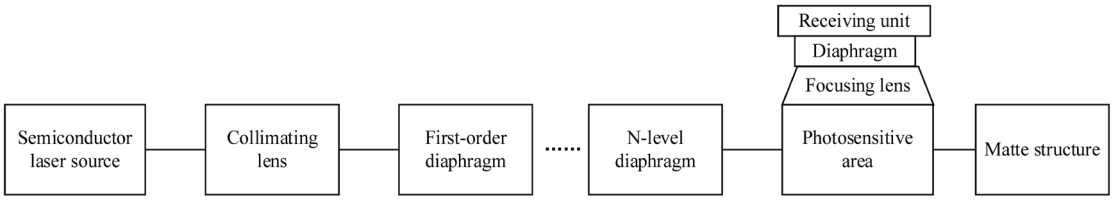

Fig. 6. Components of particle detection module.

particles. As shown in Fig. 7, an optical lens, an aerosol generator, a temperature control unit, and a smart touchscreen are integrated in the standard smoke chamber, enabling the simulation of environments with specific wind speeds, temperatures, and initial solid-particle concentrations.

The response of the solid-particle sensor unit is evaluated by releasing aerosol gases with varying parameters. If a linear relationship can be fitted between the environmental solid-particle concentration parameters and the voltage output by the particle detection module, this validates the effectiveness of the thermally released nanoparticles detection module designed in this study.

At an ambient temperature 23 ℃ and a wind speed of 0, the experiment simulated varying concentrations of solid-state particles in the environmental gas: 0, 5, 10, 15, ..., 290, 295, 300, 305, 310, 315, and 320 million particles per cubic centimeter (particles/cc). The voltage response of the signal amplification unit in the smoke detection module was recorded and analyzed under these different particle concentration scenarios.

Following multiple trials under the above experimental design, the voltage responses of the smoke detection module at various solid-particle concentrations are plotted in Fig. 8. The orange discrete points represent the actual voltage responses of the particle detection module under varying solid-particle concentrations. The analysis revealed that the voltage response increases linearly with solid-particle concentration in the environmental gas. The black straight line represents the theoretical voltage response curve obtained by fitting by the least squares method. In practice, a linear relationship exists between the environmental solid-particle concentration and the voltage response of the sensor unit.

The linear relationship between the solid-particle concentration and the voltage response, validated through prior experiments, confirms the effectiveness of the particle detection module developed in this study. Furthermore, this linear relationship enables the numerical calibration of the particle detection module, facilitating the conversion between the voltage response and the solid-particle concentration.

Fig. 7. (Color online) Smoke chamber.

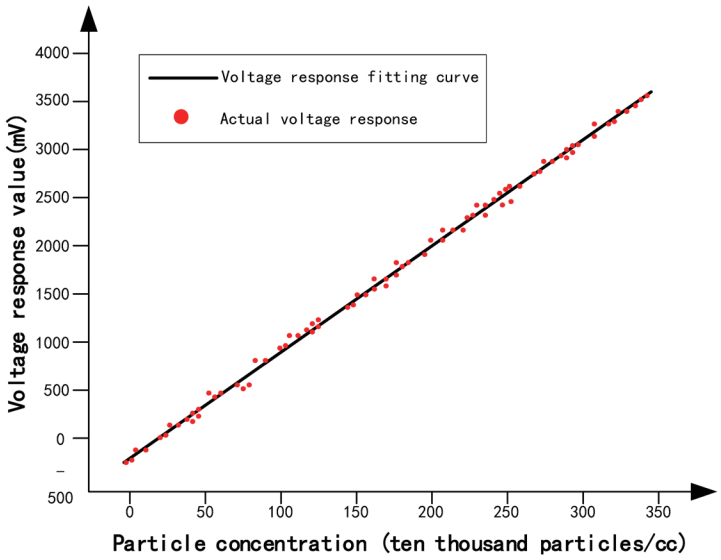

Fig. 8. (Color online) Test results of particle detection module.

4.2.2 False alarm test of the device

The detection target of this device is small-diameter nanoparticles. However, in wind farm environments, components such as dust and water mist may exhibit similar physical characteristics. To ensure reliability, anti-misfire tests were conducted to evaluate the device's capability to distinguish between target nanoparticles and these interfering factors.

A. False alarm test for water mist detection

Under ambient temperature conditions, the device's false alarm behavior in environments with water mist was tested, as shown in Fig. 9. A humidifier was used to generate mist within the test chamber. The relative humidity (% RH) was incrementally adjusted to 54% RH, 60% RH, 70% RH, 80% RH, and 90% RH, and the device's alarm status was monitored at each humidity level. A heating platform was used to vaporize pure water and produce mist. During this process, both the real-time humidity data displayed by the device and its alarm status were recorded and analyzed.

During the humidifier test, the monitoring and warning device did not trigger any alarms at test chamber humidity levels of 54, 60, 70, 80, and 90% RH. Similarly, in the heating platform test, the device remained alarm-free at humidity levels of 51.8, 56.9, 63.6, 68.7, and 69.6% RH. Therefore, neither the mist generated by the humidifier nor the water vapor produced by the heating platform caused false alarms in the monitoring system.

B. Tests of false alarm caused by dust

Under ambient temperature conditions, the device's false alarm behavior in dusty environments was evaluated, as shown in Fig. 10. During the experiment, lime powder particles were sprayed near the sampling tube of the device to simulate dust conditions, with five trials conducted. To isolate the effect of the filter core structure (installed at the sampling end of the tube), two experimental groups were tested: the device with the filter core installed (Group 1) and the device with the filter core removed (Group 2).

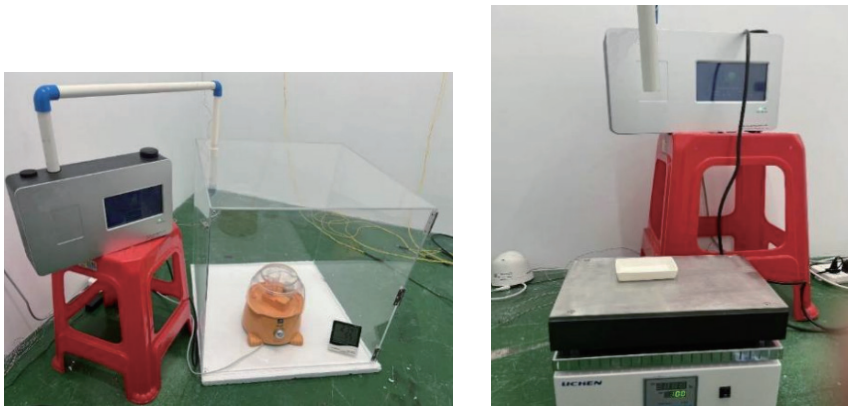

Fig. 9. (Color online) Tests of false alarm caused by water mist.

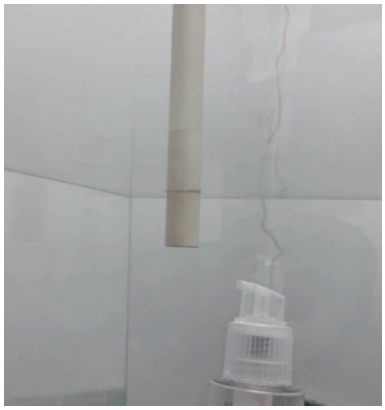

Fig. 10. (Color online) Tests of false alarm caused by dust.

We used a spray bottle (bottom of Fig. 10) to spray lime powder and pressed the button manually to spray once. During all five trials, the monitoring and warning device did not trigger any alarms. Since the lime powder particles sprayed into the environment share similar properties to dust particles, it can be concluded that dust and similar particulates do not induce false alarms in the monitoring system.

From the experimental results, the online thermal hazard monitoring device developed in this study for wind farm electrical equipment has demonstrated robust resistance to interferences from dust and water mist. This capability ensures reliable operation in environments where these common particulates or aerosols may be present.

4.3 Discussion

In this section, the thermal hazard monitoring device was designed. We adopted the Mie scattering theory to design a nanoparticle detection module, gave design principles, and provided components of the nanoparticle detection module. Before the device was applied, functional (solid-state nanoparticle detection) and anti-false alarm tests were conducted.

In the experiment on the nanoparticle detection performance of our developed device, we utilized a standard smoke chamber to simulate thermally released nanoparticles emitted from target materials. From the experiment, we can observe the linear relationship between the solid-particle concentration and the voltage output of the nanoparticle detection module, which validates the effectiveness of the thermally released nanoparticle detection module of this device. Moreover, we used this linear relationship to achieve the conversion between voltage response and solid-particle concentration. This means that the designed thermal hazard monitoring device can measure the solid-particle concentration accurately.

Considering the interferences from dust and water mist in the wind farm environment, to ensure reliability, anti-misfire tests were conducted to evaluate the device's capability to distinguish between target particles and these interfering factors. Experiments have shown that the equipment is robust against interferences in simulated water mist environments. Moreover, in the simulated dust environment, no false alarms were triggered by the equipment.

5. Conclusions

To achieve the warning of thermal hazards in wind farm electrical equipment, we proposed the development of a thermal hazard monitoring system for wind turbines based on nanoparticle detection. First, we introduced commonly used methods for early fire warning, and we then analyzed and investigated typical thermal hazard materials in wind farms. An experimental platform was established, and four representative flammable materials from wind turbines were selected as experimental samples. The concentration changes of particles of various diameters during the entire process from overheating to the combustion of these four samples were observed. On the basis of these observations, the characteristic nanoparticles of thermal hazards were identified, namely, thermally released nanoparticles with diameters smaller than 0.3 μm. The detection and alarm thresholds for these nanoparticles in wind turbine thermal hazard monitoring were determined.

On the basis of experimental results, a thermal hazard monitoring device for wind turbines using nanoparticle detection was developed. The design principles of the device were introduced, followed by tests of the effectiveness of the developed system. Anti-interference tests were also conducted to evaluate its performance in the presence of water mist and dust interferences.

The test results showed that the developed device achieves high alarm accuracy and effectively prevents false alarms caused by water mist and dust interferences. It is therefore suitable for broad applications in thermal hazard monitoring and early fire warning systems for wind turbines, ensuring reliable operation under complex environmental conditions. The device developed in this study is currently used in fire monitoring systems for multiple wind farms.

References

1 F. You, M. S. Rokonuzzaman, K. S. Rahman, and W. S. Tan: Heliyon **9** (2023) e19664. https://doi.org/10.1016/j.heliyon.2023.e19664

2 R. G. Deshagoni, T. Auditore, R. Rayudu, and C. P. Moore: IEEE Trans. Ind. Appl. **55** (2019) 6585. https://doi.org/10.1109/TIA.2019.2931866

3 N. Wang, Z. Cheng, F. You, Y. Zhang, Z. Wang, C. Zhuang, Z. Wang, G. Ling, Y. Pan, J. Wang, and J. Ma: J. Therm. Anal. Calorim. **149** (2024) 10335. https://doi.org/10.1007/s10973-024-13462-4

4 J. H. Kim, S. H. Park, S. J. Park, B. J. Yun, and Y. S. Hong: Energies **16** (2023) 5176. https://doi.org/10.3390/en16135176
5 Y. Lee, G. Lee, J. Yang, J. Park, and D. Baek: Eng. Fail. Anal. **107** (2020) 104218. https://doi.org/10.1016/j.engfailanal.2019.104218
6 W. Sun, W. Lin, F. You, C. Shu, and S. Qin: Renew. Energy **140** (2019) 62. https://doi.org/10.1016/j.renene.2019.03.045
7 B. Rengel, E. Pastor, and E. Planas: Fire Technol. **53** (2017) 1933. https://doi.org/10.1007/s10694-017-0664-0
8 A. Wan, C. Du, W. Gong, C. Wei, K. AL-Bukhaiti, S. Ji, S. Ma, F. Yao, and L. Ao: Energies **17** (2024) 2330. https://doi.org/10.3390/en17102330
9 C. Zhou, Z. Cao, G. Wei, and K. Wu: J. Electr. Eng. Technol. **18** (2023) 679. https://doi.org/10.1007/s42835-022-01178-0
10 J. Han, W. Chen, A. Yu, and J. Yi: Front. Mater. **6** (2019) 250. https://doi.org/10.3389/fmats.2019.00250
11 J. Yi, W. Chen, J. Han, and D. Chen: Sens. Actuators, B **287** (2019) 364. https://doi.org/10.1016/j.snb.2019.02.025
12 H. Xiong, J. Li, W. Li, X. Jiang, B. Xiang, and Z. Liu: Front. Energy Res. **11** (2023) 1091298. https://doi.org/10.3389/fenrg.2023.1091298
13 Y. Wang, Q. Li, J. Zhang, C. Yin, Q. Zhang, Y. Shi, and H. Men: Sens. Actuators, B **423** (2025) 136801. https://doi.org/10.1016/j.snb.2024.136801
14 H. Fu, L. Qiu, Y. Ai, B. Yang, and F. Du: Sens. Mater. **6** (2025) 2185. https://doi.org/10.18494/SAM5604
15 C. Li, J. Chen, Z. Pu, F. Tao, J. Liu, X. Tan, L. Hu, and J. Cao: Front. Energy Res. **10** (2022) 836588. https://doi.org/10.3389/fenrg.2022.836588
16 X. Chen, G. Huang, X. Gao, S. Ou, Y. Li, and I. M. Hezam: Appl. Sci. **11** (2021) 8922. https://doi.org/10.3390/app11198922
17 J. Li, F. Ai, C. Cai, H. Xiong, W. Li, X. Jiang, and Z. Liu: Energy Rep. **9** (2023) 361. https://doi.org/10.1016/j.egyr.2023.05.150
18 Z. Pu, W. Zhao, Y. Xiong, X. Shi, and C. Fang: J. China Three Gorges Univ. (Nat. Sci.) **43** (2021) 88 (in Chinese). https://doi.org/10.13393/j.cnki.issn.1672-948X.2021.01.016
19 J. Li: Electr. Eng. **02** (2025) 13 (in Chinese). https://doi.org/10.19768/j.cnki.dgjs.2025.02.005
20 C. F. Bohren and D. R. Hufm: Absorption and Scattering of Light by Small Particles (Wiley, New York, 1983).
21 W. H. White, E. S. Macias, and R. C. Nininger: Atmos. Environ. **28** (1994) 909. https://doi.org/10.1016/1352-2310(94)90249-6
22 S. V. Amarantov and S. V. Peters: Crystallogr. Rep. **68** (2023) 515. https://doi.org/10.1134/S1063774523600217
23 Z. Wang, T. Liu, H. Qiu, and M. Huang: Opt. Express **31** (2023) 19867. https://doi.org/10.1364/OE.491421
24 J. C. G. Martin, D. Guirado, E. Zubko, J. Escobar-Cerezo, and O. Munoz: J. Quant. Spectrosc. Radiat. Transfer **241** (2020) 106745. https://doi.org/10.1016/j.jqsrt.2019.106745
25 D. Chicea, A. S. Doroshkevich, and A. Lyubchyk: Sensors **22** (2022) 3871. https://doi.org/10.3390/s22103871

About the Authors

Fuhao Du received his M.S. degree in electrical engineering from Wuhan University in Wuhan, China, in 2016. He is an engineer at the Wuhan Cloud Scout Science & Technology Co., Ltd. in Wuhan, China. His current research interests focus on electric fire detection. (13971150995@163.com)

Lun Liu received his M.S. degree in electrical and electronic engineering from Huazhong University of Science and Technology in Wuhan, China, in 2015. He is an engineer at the Wuhan Cloud Scout Science & Technology Co., Ltd, in Wuhan, China. His current research interests focus on electric fire detection. (liulun@whyunzhen.com)

Man Xu received her M.S. degree in power engineering and engineering thermophysics from Zhejiang University of Technology in Hangzhou, China, in 2020. She is an engineer at the Wuhan Cloud Scout Science & Technology Co., Ltd, in Wuhan, China. Her current research interests focus on electric fire detection. (17816038133@163.com)